LAWRENCE
LIVERMORE
NATIONAL
LABORATORY

UCRL-JRNL-206133

Probing the population of the spin-orbit split levels in the actinide 5f states

K. Moore, G. van der Laan, J. Tobin, B. Chung, M. Wall, A. Schwartz

August 19, 2004

Ultramicroscopy

Ultramicroscopy: PDF for review

Journal	Ultramicroscopy
Article ID	ULTRAM_91
Title	Probing the population of the spin-orbit split levels in the actinide 5f states
Version	1
Article type	Full-length article
Submitted	21 Mar 05

Files submitted

Name	Fig No	Format	Use	Description
UM text(Moore).doc		Manuscript (Microsoft Word)		text
Fig1(Moore).tif	1	Figures (TIFF)	Yes	
Fig2(Moore).tif	2	Figures (TIFF)	Yes	
Fig3(Moore).tif	3	Figures (TIFF)	Yes	
Fig4(Moore).tif	4	Figures (TIFF)	Yes	

Probing the population of the spin-orbit split levels in the actinide 5*f* states

K.T. Moore,[1,*] G. van der Laan,[2] J.G. Tobin,[1] B.W. Chung,[1] M.A. Wall,[1] A.J. Schwartz,[1]

[1]*Lawrence Livermore National Laboratory, Livermore, California 94550, USA*

[2]*Magnetic Spectroscopy Group, Daresbury Laboratory, Warrington, WA4 4AD, UK*

Spin-orbit interaction in the 5*f* states is believed to strongly influence exotic behaviors observed in actinides metals and compounds. Understanding these interactions and how they relate to the actinide series is of considerable importance. To address this issue, the branching ratio of the white-line peaks of the $N_{4,5}$ edges for the light actinide metals, α-Th, α-U, and α-Pu were recorded using electron energy-loss spectroscopy (EELS) in a transmission electron microscope (TEM) and synchrotron-radiation-based x-ray absorption spectroscopy (XAS). Using the spin-orbit sum rule and the branching ratios from both experimental spectra and many-electron atomic spectral calculations, accurate values of the spin-orbit interaction, and thus the relative occupation of the j = 5/2 and 7/2 levels, are determined for the actinide 5*f* states. Results show that the spin-orbit sum rule works very well with both EELS and XAS spectra, needing little or no correction. This is important, since the high spatial resolution of a TEM can be used to overcome the problems of single crystal growth often encountered with actinide metals, allowing acquisition of EELS spectra, and subsequent spin-orbit analysis, from nm-sized regions. The relative occupation numbers obtained by our method have been compared with recent theoretical results and show a good agreement in their trend.

*Contact Author

Tel: 925-422-9741

Fax: 925-422-6892

Email: moore78@llnl.gov

1. Introduction

A recent surge of interest in the actinides has occurred, driven by the variety of exotic behaviors exhibited in 5*f* metals and compounds [1-11], such as the discovery of Pu-based superconductivity [8-10], and the unique phonon dispersion observed in α-U [6,7] and δ-Pu [3-5]. Along the actinide series a volume anomaly occurs near Pu, due to a change in the bonding behavior of the valence states (see Figure 1 [11]). While the *s* and *d* electron orbitals are broad and strongly overlapping, the 5*f* states are narrower and have less overlap. In the lightest elements of the actinide series the *f* electrons are strongly bonding, while in the heavier actinides they are not bonding, creating a jump in volume between α-Pu and α-Am of 40%. Since the *s* and *d* valence states do not change much along the actinide series, the 5*f* states are of particular interest. The spin-orbit interaction for these heavy elements may likely be the culprit for the above mentioned exotic behaviors, and is the topic of this paper.

Using the spin-orbit sum rule and the branching ratios from both experimental spectra and many-electron atomic spectral calculations, we have determined the relative occupation of the **j** = 5/2 and 7/2 levels, and thus the expectation value of the spin-orbit interaction, for the actinide 5*f* states. Experimental spectra were acquired by electron energy-loss spectroscopy (EELS) in a transmission electron microscope (TEM) and by synchrotron-radiation-based x-ray absorption (XAS). Theoretical spectra were produced using many-electron calculations, where spin-orbit, Coulomb, and exchange interactions are treated on equal footing. These data show that we can obtain the value of the spin-orbit interaction per hole from the branching ratio of the actinide $N_{4,5}$ EELS or XAS spectra, and in turn examine how the 5*f* states of each metal relate to the various coupling schemes.

The ability of EELS in a TEM to replicate synchrotron-radiation-based XAS spectra is of great importance to the actinides. These metals have numerous solid allotropic phases [12] and growing the large single crystals that are suitable for synchrotron-radiation-based XAS is often extremely difficult. The high spatial resolution of a field-emission-gun TEM circumvents the need for large single crystals, allowing us to record spectra from nm-sized areas of a sample. This in turn allows us to examine the spin-orbit interaction of the valence states in actinide metals and compounds using the branching ratio and the spin-orbit sum rule.

The outline is as follows. In Section 2 we will give a brief, but self-contained, introduction into coupling schemes, spin-orbit interaction, and the branching ratio of core-level spectra. In Section 3 we will give the experimental details for EELS and XAS measurements. In Section 4 we will apply the spin-orbit sum rule to the spectra of the light actinides. With these data we will illustrate that the spin-orbit sum rule works quite well for the actinide 5*f* states, needing little or no correction factor. Conclusions are drawn in Section 5.

2. Spin-orbit interaction and branching ratio

In the Hamiltonian used for electronic structure calculations, there are two standard ways to couple the angular momenta of multi-electronic systems: Russell-Saunders (**LS**) and **jj** coupling. In atoms where the spin-orbit coupling is weak compared to the Coulomb and exchange interaction, the orbital angular momenta **l** of individual electrons are coupled to a total orbital angular momentum **L** and likewise the spin angular momenta **s** are coupled to a total **S**. Then, **L** and **S** are coupled to form the total angular momentum **J**. This approach simplifies the calculation of the Coulomb and exchange interactions, which commutate with **L**, **S**, and **J**, and hence are diagonal in these quantum numbers. For heavier elements with larger nuclear charge, there is also an important contribution from the spin-orbit interaction. This interaction is diagonal in **j** and **J**, but not in **L** and **S**. Therefore, in the **jj** coupling scheme, the spin and orbital angular momenta, **s** and **l**, of each electron are coupled to form individual electron angular momenta **j** and then the different **j** are coupled to give the total angular momentum **J**. Both schemes are equally viable. In a many-electron system, the basis states obtained in **LS** and **jj** coupling can be changed into each other by using a recoupling transformation matrix. For purposes of numerical calculation of the energy levels and the spectral intensities by diagonalization of the Hamiltonian matrix it is immaterial what pure-coupling representation is used. The solution obtained by exact matrix diagonalization is known as intermediate coupling. Note that for a one-electron system there is no difference between **LS** and **jj** coupling. Unfortunately, the one-electron approach commonly used to calculate the electronic structure of materials does not take full advantage of the recoupling techniques that are available for many-electron systems.

For convenience, the atomic ground state is often expressed in a pure-coupling representation. It is known that **LS** coupling holds quite well for transition metals (in the

absence of crystal field) and for rare earth metals [13]. These systems exhibit a Hund's rule ground state with maximum **S** and **L**, which are coupled by spin-orbit interaction antiparallel or parallel to each other for less or more than half filled shell, respectively, resulting in **J**=|**L**-**S**| or **J**=**L**+**S**, respectively. However, for the 5*f* states of the actinides the spin-orbit interaction is much stronger, giving a significant mixing of the Hund's rule ground state by other **LS** states with the same **J** value. Hence, the **LS** states will be less pure and there is a tendency towards the **jj** coupling limit [14,15]. The choice of the coupling limit has profound implications for the expectation value of the spin-orbit interaction, as well as for any other orbital-related interactions, such as the orbital magnetic moment. We will concentrate here on the spin-orbit interaction, the trends for the other spin-orbital coupled tensors can be found in [16].

Defining the angular part of the expectation value of the spin-orbit interaction as $\langle w^{110} \rangle = (ls)^{-1} \langle l \cdot s \rangle$, we can easily evaluate its value in **LS** and **jj** coupling. For a pure **LSJ** level of a valence l shell (l=1, 2 and 3 for p, d, and f shell, respectively) we have

$$\langle w^{110} \rangle = \frac{J(J+1) - L(L+1) - S(S+1)}{lw}, \qquad (1)$$

where $w = n$ for $n \le 2l+1$ and $w = -n_h$ for $n > 2l+1$, with n and n_h the number of electrons and holes, respectively, in the l shell, and $n + n_h = 4l + 2$.

Spin-orbit interaction splits the l shell ($l \neq 0$) into two levels $j_1 = l - \frac{1}{2}$ and $j_2 = l + \frac{1}{2}$, which have a degeneracy of $2j_1 + 1 = 2l$ and $2j_2 + 1 = 2l + 2$, respectively. Every j_1 electron contributes $-(l+1)/l$ to the spin-orbit interaction $\langle w^{110} \rangle$, while every j_2 electron contributes a value of 1. Due to the dominant spin-orbit interaction in the **jj** coupling limit, the j_1 levels are filled first and only when these are completely full can the j_2 levels begin to fill. Therefore we obtain

$$\langle w^{110} \rangle = -\frac{l+1}{l} n, \text{ for } n \le 2l, \qquad (2)$$

$$\langle w^{110} \rangle = -n_h, \text{ for } n > 2l. \qquad (3)$$

Since the spin-orbit interaction is diagonal in **j**, one can derive a simple equation that is generally valid for any state in any coupling scheme (and hence in intermediate coupling), namely

$$\left\langle w^{110} \right\rangle = n_{j_2} - \frac{l+1}{l} n_{j_1} \ , \qquad (4)$$

where n_{j_1} and n_{j_2} are the occupation numbers of the j_1 and j_2 levels, respectively, and the total number of electrons is $n = n_{j_1} + n_{j_2}$.

For core-valence transitions such as EELS and XAS, there exists what is called a branching ratio [16-18], which can function as a local probe for the spin-orbit interaction of the valence electrons for a material. Transition metals, rare earths, and actinides exhibit high-intensity peaks at the threshold of absorption edges, often called white lines, which are due to electric-dipole transitions from core levels to unoccupied states in the valence band.

These spectra are split by the large core spin-orbit interaction into two manifolds $j_+ = c + \frac{1}{2}$ and $j_- = c - \frac{1}{2}$. The transition probabilities from the core levels j_+ and j_- to the valence levels j_1 and j_2 are different. Because the total spin-orbit interaction is linear in the number of j_1 and j_2 electrons, the branching ratio is linear in the valence spin-orbit interaction per hole. The branching ratio is a measurement of the areas beneath these white line peaks: $B = A_{j_+} / (A_{j_+} + A_{j_-})$. For the electric-dipole transition from a core level with orbital quantum number c=l-1 to a valence state l, we find the following relation [16-19],

$$\frac{\left\langle w^{110} \right\rangle}{n_h} = -\frac{2c+1}{c}(B - B_0), \qquad (5)$$

where B_0 is the branching ratio in the absence of valence spin-orbit interaction.

The branching ratio depends not only on the ground-state spin-orbit interaction but also on the core-valence interactions, which are mixing the j_+ and j_- core levels [19]. If we can neglect these core-valence interactions, then B_0 is equal to the statistical value of $B_0 = (c+1)/(2c+1)$ and Equation (5) is exact. Equation (5) can then be considered as a sum rule in the same way as the spin and orbital magnetic moment sum rules in x-ray magnetic circular dichroism (XMCD) [20,21].

When core-valence interactions do play a role, Equation (5) is no longer exact and B_0 is affected. Considering the periodic table, there are numerous trends observed along the different transition-metal series due to diverse valence-electron behavior [17]. For 3*d* transition metals, the application of the spin-orbit sum rule for the $L_{2,3}$ branching ratio is severely hampered by the large (2*p*,3*d*) exchange interaction that is of similar size as the 2*p* spin-orbit interaction [17]. The same is true of the $M_{4,5}$ edges of the lanthanides, where the (3*d*,4*f*) exchange interaction is quite strong compared to the 3*d* core spin-orbit interaction [22]. On the other hand, for the $L_{2,3}$ edges of 4*d* and 5*d* transition metals, associated with the deep 2*p* core level, the sum rule is expected to hold quite well. However, even in the case of the rare earth the trend in the branching ratio can be used the obtain the relative population of spin-orbit split states, as was demonstrated for Ce systems [23].

The situation is favorable for the $M_{4,5}$ and $N_{4,5}$ edges of the actinides, given the small exchange interactions between the 3*d* and 4*d* core levels and the 5*f* states [15]. The latter result is rather surprising, since in spite of the fact that the Th 4*d* core level is more shallow than the Zr 2*p* of Hf 2*p* and lies in between the Ti 2*p* and La 3*d*, the core-valence interactions do not spoil the sum rule for the 5*f* states. Our calculations showed that B_0 varies between only 0.59 and 0.60 for the light actinides (see Table I) and, therefore, are very close to the statistical ratio [15]. This means that the EELS and XAS branching ratios depend almost solely on the 5*f* spin-orbit expectation value per hole, and thus we now have an unambiguous probe for the 5*f* spin-orbit interaction.

3. Experimental procedures

EELS experiments were performed using a Phillips CM300 field-emission-gun TEM, equipped with a Gatan imaging filter for the collection of spectra. The electron excitations were justified as electric-dipole transitions because the accelerating voltage of the TEM was 300 keV, and much larger than the energy of the $N_{4,5}$ transitions for Th, U, and Pu [24]. The similarity between high-energy EELS spectra and synchrotron-radiation-based XAS has been well known for some time, and was recently validated for *f*-electron systems for the case of Ce [25]. EELS spectra were recorded in imaging mode using a collection angle of 6 mrad, which allowed the 000 beam and the first-order reflections to contribute to the spectra. All spectra were reproduced

numerous times using a sample thickness of approximately 0.5 inelastic mean free path, as calculated by the zero-loss and plasmon peaks. Multiple spectra were recorded, aligned, and summed to optimize the signal-to-noise ratio and to maintain optimal energy resolution of about 1 eV. Samples were 99.9% pure and were prepared via either electropolishing or ion milling. While Th and U could be handled directly, all Pu work was performed in a glove box, and the samples were transported in a vacuum-transfer holder due to the toxic nature of the metal (for full sample preparation procedures, see [26]). The XAS spectra were collected at the Advanced Light Source in total-electron-yield mode, using a 30 mg sample of purified α-Pu (details are provided elsewhere [27]).

4. Results and Discussion

The $N_{4,5}$ EELS edges for α-Th, α-U, and α-Pu are shown in Figure 2, each accompanied by a single-crystal diffraction pattern that confirms the phase being examined. An XAS spectrum from α-Pu is also presented [27,28]. The spin-orbit split $4d_{3/2}$ and $4d_{5/2}$ manifolds are clearly resolved for each metal as a pair of white lines. No fine structure is resolved for either edge due to the intrinsic core-hole lifetime broadening of ~2 eV [16,29]. Along the actinide series from Th to Pu the $4d_{3/2}$ peak progressively reduces in intensity due to the fact that selection rules govern that a $d_{3/2}$ core-level electron can only be excited into an $f_{5/2}$ level. Therefore, the steady decrease in intensity of the $4d_{3/2}$ peak in Figure 2 indicates a progressive filling of the $5f_{5/2}$ level along the actinide series, as previously observed [14].

We may now use the areas beneath the N_4 ($4d_{3/2} \rightarrow 5f_{5/2}$) and N_5 ($4d_{5/2} \rightarrow 5f_{5/2,7/2}$) white-line peaks to calculate the branching ratio (B), which is summarized in Table I and plotted in Figure 3 as a function of the number of $5f$ electrons (n). The branching ratio is defined as

$$B = \frac{A_{5/2}}{A_{5/2} + A_{3/2}} \quad , \qquad (6)$$

where $A_{5/2}$ and $A_{3/2}$ are the areas within the $d_{5/2}$ and $d_{3/2}$ peaks, respectively. Figure 3 contains the branching ratios for the EELS and XAS spectra in Figure 2, the α-U XAS from Kalkowski *et al.* [29], and the spectral calculations using a many-electron atomic model [30] in intermediate coupling. Here we use n = 0.6 for Th, n = 3 for U, and n = 5 for Pu. Examination of Figure 3 shows that the calculated branching ratios for n = 0 to 5 exhibit a roughly linear dependence.

The experimental branching ratios for all three metals fall near the line with Th and Pu being almost directly on. We may now consider the branching ratios more analytically, paying particular attention to how the branching ratio can give us information on the coupling scheme of the 5*f* states.

For the transition from the core *d* to the 5*f* states, the spin-orbit sum rule is given as [16],

$$B = B_0 - \frac{2}{5}\frac{\langle w^{110}\rangle}{n_h} \quad , \qquad (7)$$

where

$$\langle w^{110}\rangle = n_{7/2} - \tfrac{4}{3} n_{5/2} \quad , \quad (8)$$

$$n_h = 14 - \left(n_{7/2} + n_{5/2}\right) \quad , \quad (9)$$

with $n_{7/2}$ and $n_{5/2}$ are the electron occupation numbers of the $5f_{7/2}$ and $5f_{5/2}$ levels, respectively.

The experimental values of $\langle w^{110}\rangle$ were obtained from Equation (7) by substitution of the measured *B* values, together with the statistical value 3/5 for B_0. Utilizing Equation (8) and (9) gives the values for $n_{5/2}$ and $n_{7/2}$ shown in Table I. If we would use the B_0 values (0.59 to 0.60) as obtained from the calculation, we obtain $\langle w^{110}\rangle^{C}$, where the superscript C stands for "corrected". Using these values of B_0 with the experimental data causes only a small effect, as shown in Table I. The corrected experimental values, $\langle w^{110}\rangle^{C}$, are plotted in Figure 4, along with the calculated results from [16] for the two coupling limits: **LS** (short dash line), **jj** (long dash line), and for intermediate coupling (solid line). Since it takes at least two electrons to tangle, there is no difference between the various coupling schemes for one electron. This is in fact observed for Th, which has less than one electron in the 5*f* shell. The results for U are well approximated by the **LS** coupling limit, while the Pu $\langle w^{110}\rangle^{C}$ values are almost directly on the intermediate coupling curve. This explains why band calculations such as unmodified local density approximation (LDA) work well with U [31], but fail for Pu unless augmented with the generalized gradient approximation with spin-orbit coupling [32].

Another (but completely equivalent) way to look at the spin-orbit interaction is to examine the occupation of the $5f_{5/2}$ and $5f_{7/2}$ levels, shown in Table I, together with the various predictions for the intermediate coupling case; the statistical distribution in the absence of spin-orbit interaction and the **jj** coupling model (c.f. Equation (2)). The calculations in intermediate coupling

were obtained from relativistic Hartree-Fock calculations using Cowan's code [30]. From Table I we see the remarkable fact that for U and Pu the occupation of the **j**=7/2 level is about the same but that the two extra electrons of Pu go entirely in the **j**=5/2 level. The $f_{5/2}$ and $f_{7/2}$ occupation numbers of Th and Pu are consistent with the intermediate coupling case, while those of U are consistent with the intermediate case, consistent with previous results [31].

Returning to Figure 1, our data support the hypothesis that the upturn that occurs in the atomic volume just prior to the large volume increase between α-Pu and α-Am is due to the 5*f* spin-orbit interaction. This is in fact supported by the calculations of Pénicaud [33] and by previous experimental results for the $5d \rightarrow 5f$ transition in Th, U, and Pu [14]. We can directly compare the numbers for $n_{5/2}$ and $n_{7/2}$ in our Table I with those from Figure 5 of Pénicaud [33], which are shown in Table II. These numbers were attained by extracting the values of $n_{5/2}$ and $n_{7/2}$ from Pénicaud and calculating $\langle w^{110} \rangle$ using Equation (8). The trend is in agreement with what we find experimentally, although Pénicaud's calculated numbers for $n_{5/2}$ and (absolute $\langle w^{110} \rangle$) are systematically too low. Th and Pu give a statistical distribution in the calculated model, while we already observe a strong preference for $n_{5/2}$ (i.e. narrow band). In agreement between our experiment and Pénicaud's calculations is the fact that between U and Pu the $n_{7/2}$ count remains almost constant while the $n_{5/2}$ count grows. The Pénicaud model shows that $5f_{5/2}$ states hybridize stronger than the $5f_{7/2}$ states, and this hybridization decreases the equilibrium volume.

A final point of interest is in the Appendix of Reference 23, where Figure A1 gives the results of an Anderson Impurity calculation that shows nicely how the $f_{5/2}$ and $f_{7/2}$ concentrations depend on the hybridization and the relative position of the Fermi level. In order to obtain a large $f_{7/2}$ concentration the hybridization has to be large, but furthermore the $f_{5/2}$ has to be above the Fermi level. Thus, when the $f_{5/2}$ density of states goes gradually through the Fermi level, going from U to Pu, the relative $f_{7/2}$ concentration decreases.

5. Conclusions

In conclusion, our results show that: (1) The spin-orbit sum rule works excellently for the actinide 5*f* states. This means we now have an unambiguous probe for the 5*f* spin-orbit

interaction. (2) The spin-orbit sum rule works not only for XAS, but also for EELS obtained in a TEM. This is quite powerful because the small probe of a TEM can be used to circumvent the inability to grow large single crystals of certain materials, which are often needed for synchrotron-radiation-based XAS. One can then analyze the spin-orbit interaction of the valence states of a material using EELS. (3) Because of its low 5*f* occupation (less than an electron) the Th result is consistent with all different angular momentum coupling schemes: **LS**, **jj**, and intermediate. (4) Uranium exhibits an **LS** scheme, matching previous experimental results. (5) Pu results clearly point to the necessity of an intermediate scheme.

We hope that these results entice more electron microscopists and EELS experts to utilize the spin-orbit sum rule, a tool that hitherto has been primarily used by the synchrotron radiation community.

6. Acknowledgements

This work was performed under the auspices of the U.S. Department of Energy by University of California Lawrence Livermore National Laboratory under contract number W-7405-Eng-48, with support from Lawrence Berkeley National Laboratory under contract number DE-AC03-76SF00098. The Advanced Light Source and the Spectromicroscopy Facility (Beamline 7.0) have been built and operated under funding from the Office of Basic Energy Science at Department of Energy. The authors wish to thank Jason Lashley and Michael Blau for the Pu samples, and R. Schultz, D. Shuh, J. Terry, J.D. Farr, T. Zocco, K. Heinzelman, and E. Rotenberg for help with the Pu data collection at the Advanced Light Source.

References

1. R.C. Albers, *Nature* **410**, 759 (2001).
2. S.Y. Savrasov, G. Kotliar, E. Abrahams, *Nature* **410**, 793 (2001).
3. G. Lander, *Science* **301**, 1057 (2003).
4. X. Dai, S.K. Savrasov, G. Kotliar, A. Migliori, H. Ledbetter, E. Abrahams, *Science* **300**, 953 (2003).

5. J. Wong, M. Krisch, D.L. Farber, F. Occelli, A.J. Schwartz, T.C. Chiang, W. Wall, C. Boro, R.Q. Xu, *Science* **301**, 1078 (2003).
6. G.H. Lander, E.S. Fisher, S.D. Bader, *Adv. in Phys.* **43**, 1 (1994).
7. M.E. Manley, B. Fultz, R.J. McQueeney, C. M. Brown, W. L. Hults, J. L. Smith, D. J. Thoma, R. Osborn, J. L. Robertson *Phys. Rev. Lett.* **86**, 3076 (2001).
8. J.L. Sarrao, L.A. Morales, J.D. Thompson, B.L. Scott, G.R. Stewart, F. Wastin, J. Rebizant, P. Boulet, E. Colineau, G.H. Lander, *Nature* **420**, 297 (2002).
9. I. Opahle, P.M. Oppeneer, *Phys. Rev. Lett.* **90**, 157001 (2003).
10. T. Maehira, T. Hotta, K. Ueda, A. Hasegaw, *Phys. Rev. Lett.* **90**, 207007 (2003).
11. S.S. Hecker, *MRS Bulletin* **26**, 872 (2001) and reference therein.
12. K.T. Moore, M.A. Wall, A.J. Schwartz, B.W. Chung, S.A. Morton, J.G. Tobin, S. Lazar, F.D. Tichelaar, H.W. Zandbergen, P. Söderlind, G. van der Laan, *Philos. Mag.* **84**, 1039 (2004).
13. C. Kittel, *Introduction to Solid State Physics* 5th Ed. (John Wiley and Sons, NY, 1976) page 442.
14. K.T. Moore, M.A. Wall, A.J. Schwartz, B.W. Chung, D.K. Shuh, Schulze, J.G Tobin, *Phys. Rev. Lett.* **90**, 196404 (2003).
15. G. van der Laan, K.T. Moore, J.G. Tobin, B.W. Chung, M.A. Wall, A.J. Schwartz, *Phys. Rev. Lett.* **93,** 097401 (2004).
16. G. van der Laan, B.T. Thole, *Phys. Rev. B* **53**, 14458 (1996).
17. G. van der Laan, B.T. Thole, *Phys. Rev. Lett.* **60**, 1977 (1988).
18. B.T. Thole, G. van der Laan, *Phys. Rev. B* **38**, 3158 (1988).
19. B.T. Thole, G. van der Laan, *Phys. Rev. A* **38**, 1943 (1988).
20. G. van der Laan, *J. Magn. Magn. Mater.* **156**, 99 (1996).
21. G. van der Laan, *J. Electron Spectrosc. Relat. Phenomen*. **86**, 41 (1997).
22. B.T. Thole G. Van der Laan, J.C. Fuggle, G.A. Sawatzky, R.C. Karnatak, J.M. Esteva, *Phys. Rev. B* **32**, 5107 (1985).
23. G. van der Laan, B.T. Thole, G.A. Sawatzky, J.C. Fuggle, R.C. Karnatak, J.M. Esteva, B. Lengeler, *J. Phys. C: Solid State Phys*. **19**, 817 (1986).
24. R.F. Egerton, *Electron energy-loss spectroscopy in the electron microscope*, 2nd Ed. (Plenum Press, NY, 1996) page 221.

25. K. T. Moore, B. W. Chung, S. A. Morton, A. J. Schwartz, J. G. Tobin, S. Lazar, F. D. Tichelaar, H. W. Zandbergen, P. Söderlind, and G. van der Laan, *Phys. Rev. B* **69**, 193104 (2004).
26. K.T. Moore, M.A. Wall, A.J. Schwartz, *J. Nucl. Mater.* **306**, 213 (2002).
27. J.G. Tobin, B.W. Chung, R.K. Schulze, J. Terry, J.D. Farr, D.K. Shuh, K. Heinzelman, E. Rotenberg, G.D. Waddill, G. van der Laan, *Phys. Rev. B* **68**, 115109 (2003).
28. In the raw XAS data it is possible to see the inverted Ni 2*p* white lines superimposed on the Pu 4*d* edge structure, due to a reduction of the I_0 beam by x-ray absorption in some part of the beamline optics. This Ni spectral interference was removed prior to branching ratio determination.
29. G. Kalkowski G. Kaindl, W.D Brewer, W. Krone, *Phys. Rev. B* **35**, 2667 (1987). The peak ratio of the $N_{4,5}$ edge is given in the first complete paragraph on p. 2675.
30. R.D. Cowan, *The Theory of Atomic Structure and Spectr*a (University of California Press, Berkeley, 1981).
31. P. Söderlind, *Adv. Phys.* **47**, 959 (1998).
32. P. Söderlind, *Europhys. Lett.* **55**, 525 (2001).
33. M. Pénicaud, J. Phys: Condens. Matter **9**, 6341 (1997).
34. Y. Baer, J.K. Lang, *Phys. Rev. B* **21**, 2060 (1980).
35. J.R. Naegele, Landolt-Bornstein, Group III **23B**, 183 (1994).

Table I.

The number of 5*f* electrons (n), branching ratio (B) of the actinide $N_{4,5}$ edge spectra, 5*f* spin-orbit expectation value $\langle w^{110} \rangle$, electron occupation numbers of $5f_{5/2}$ level ($n_{5/2}$) and $5f_{7/2}$ level ($n_{7/2}$), branching ratio without 5*f* spin-orbit interaction (B_0), and spin-orbit expectation value $\langle w^{110} \rangle^{C}$, corrected using the calculated B_0 value. The calculations in intermediate coupling where performed using the actual Hartree-Fock values [16]. The XAS data are from Tobin *et al.* [27] and Kalkowski *et al.* [29].

	n	B	$\langle w^{110} \rangle$	$n_{5/2}$	$n_{7/2}$	B_0	$\langle w^{110} \rangle^{C}$
Calculations in	0	0.592	0	0	0	0.592	-
intermediate coupling	1	0.634	–1.33	1	0	0.583	-
	2	0.680	–2.57	1.96	0.04	0.594	-
	3	0.723	–3.50	2.79	0.21	0.596	-
	4	0.760	–4.04	3.45	0.55	0.598	-
	5	0.817	–4.88	4.23	0.77	0.600	-
Statistical distribution	n	3/5	0	$3n/7$	$4n/7$	3/5	-
jj coupling	$n \le 6$	$\frac{3}{5}+\frac{8}{15}\frac{n}{n_h}$	$-4n/3$	n	0	3/5	-
Experiment							
EELS – Th	0.6 [a]	0.623	–0.77	0.59	0.01	0.589	–1.16
XAS - U (Kalkowski *et al.*)	3 [b]	0.676	–2.09	2.18	0.82	0.596	–2.20
EELS - U	3 [b]	0.685	–2.34	2.28	0.71	0.596	–2.45
XAS - Pu (Tobin *et al.*)	5 [c]	0.813	–4.79	4.20	0.80	0.600	–4.79
EELS - Pu	5 [c]	0.826	–5.09	4.32	0.67	0.600	–5.09

a) Reference 34 reports a Th 5*f* occupation of 0.5. However, given the Th experimental branching ratio, our calculations reveal that there must be a 5*f* occupation of ≥ 0.6 in order to have a non-negative $5f_{7/2}$ occupation.

b) Reference 35, p. 226: $n_U = 3 - \varepsilon$, assume $\varepsilon \to 0$, then $n_U \to 3$.

c) Reference 35, p. 226: $n_{Pu} = 5 - \xi$, assume $\xi \to 0$, then $n_{Pu} \to 5$.

Table II.

The number of 5*f* electrons in the **j**=5/2 ($n_{5/2}$) and **j**=7/2 ($n_{7/2}$) levels as calculated by Pénicaud [33]. Notice the high level of agreement with the trend of the values achieved in the present experiments reported in Table I.

	$n_{5/2}$	$n_{7/2}$	$\langle w^{110} \rangle$
Th	0.2	0.2	-0.07
U	1.75	1.25	-1.08
Pu	3.5	1.6	-3.07

Figure Captions

Figure 1: A plot of the Wigner-Seitz atomic radius as a function of the actinide metal series (after [11]). Notice the large jump in volume that occurs near Pu, signaling a significant change in valence electron behavior.

Figure 2: The $N_{4,5}$ ($4d \rightarrow 5f$) edges from α-Th, α-U, and α-Pu acquired by EELS in a TEM and from α-Pu acquired by XAS. A single-crystal diffraction pattern from each metal is presented, confirming the phase being examined by EELS.

Figure 3: The branching ratio (B) as a function of the number of $5f$ electrons (n) calculated in intermediate coupling. The straight line through the points is a guide to the eye. The horizontal dashed line gives the statistical value ($B_0=\frac{3}{5}$) of the branching ratio. The N_4/N_5 white line ratio for U as acquired by XAS is reported in Ref. [29].

Figure 4: (a) The spin-orbit interaction $\left\langle w^{110} \right\rangle^{C}$ (corrected for B_0) as a function of the number of $5f$ electrons (n). The three different coupling schemes are plotted: **LS** (short dash), **jj** (long dash), and intermediate coupling calculated using relativistic Hartree-Fock values (solid) [16].

Figure No: 1

Legend:

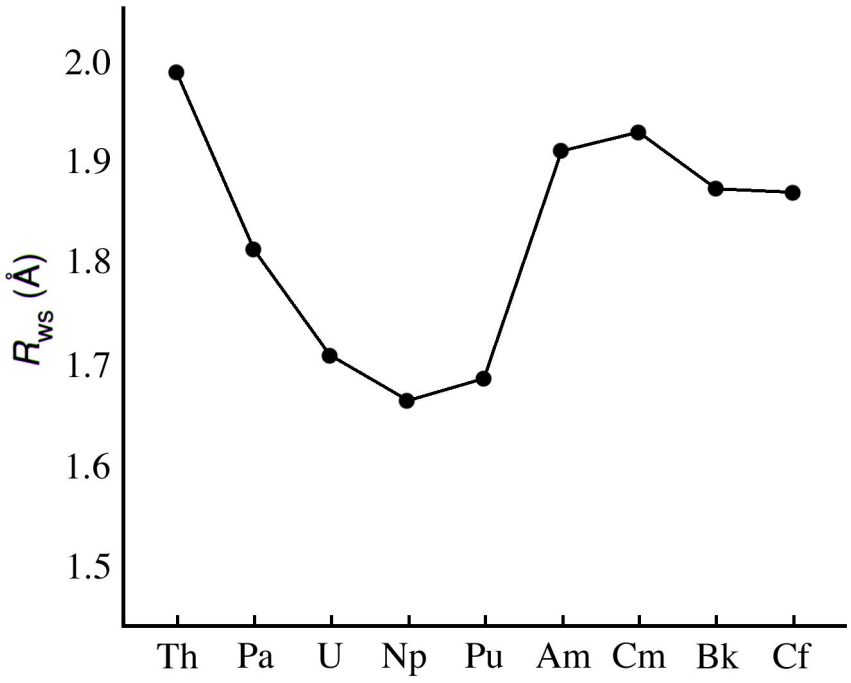

Figure No: 2

Legend:

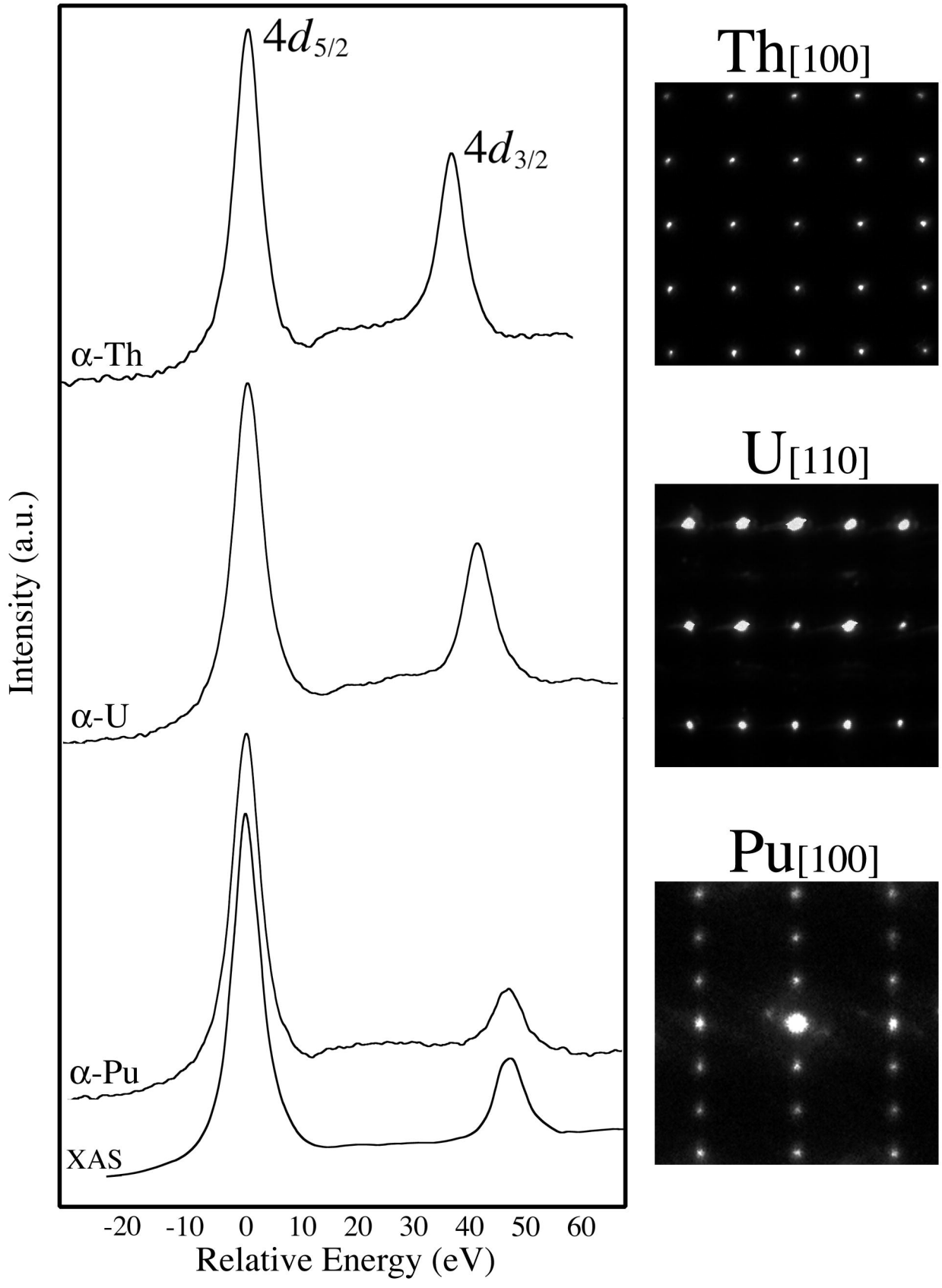

Figure No: 3

Legend:

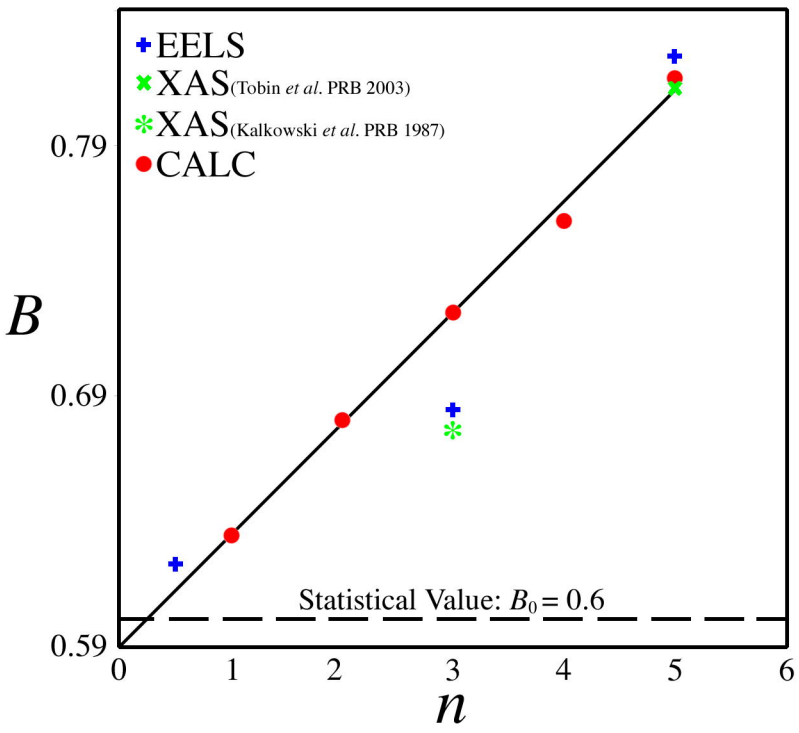

Figure No: 4

Legend: